Actinomycin D Binds to Metastable Hairpins in Single-Stranded DNA

Randy M. Wadkins,*,‡ Bogdan Vladu,‡ and Chang-Shung Tung§

Laboratory of Biophysical Chemistry, Cancer Therapy and Research Center, Institute for Drug Development, 14960 Omicron Drive, San Antonio, Texas 78245, and Los Alamos National Laboratory, Mail Stop K-710, Group T-10, Los Alamos, New Mexico 87545

Received April 29, 1998; Revised Manuscript Received June 30, 1998

ABSTRACT: We have examined the role of DNA composition in the binding of actinomycin D to single-stranded DNA. By using the fluorescent analogue 7-aminoactinomycin D, we were able to monitor binding of the drug to ssDNA with single base changes distant from the 5′-TAGT-3′ site previously determined to be a high-affinity site for actinomycin D binding (Wadkins et al. (1996) *J. Mol. Biol. 262*, 53−68). Our binding studies indicated that secondary structures in the ssDNA were likely to be responsible for binding the drug. A series of six low-melting DNA hairpins containing all or part of the 5′-TAGT-3′ binding site were synthesized. The highest T_m observed for the melting of these hairpins was 34.2 ± 0.3 °C, and it depended on the length of the stem region. These metastable hairpins were stabilized by 7-aminoactinomycin D, with the drug shifting the T_m for the drug−hairpin complex to ∼45 °C. The hairpins showed very high affinity ($K_d \sim 0.1\ \mu$M) for 7-aminoactinomycin D, with some dependence on stem length. Digestion of the hairpins in the presence and absence of drug using mung bean nuclease, which specifically interacts with the loop region of hairpin DNA, revealed that the stable hairpins (i) contain a number of non-Watson−Crick base pairs, and (ii) undergo a conformational change in the loop region upon binding 7-aminoactinomycin D. Our results suggest that stabilization of unusual hairpins by actinomycin D may be an important aspect of the potent transcription inhibition activity of this drug.

Actinomycin D (AMD[1]) is one of the most widely studied, biologically active, small molecules. The widespread interest in actinomcyin D is due to the drug's activity as an antibiotic and as an antitumor agent (reviewed in refs *1*, *2*). The drug exerts its biological activity through inhibition of transcription in a wide variety of systems (*3*−*7*). In vitro, the drug binds to double-stranded DNA (dsDNA) containing GC sites, and the high affinity and slow dissociation from these DNAs have suggested a mechanism whereby the drug blocks the progression of RNA polymerase along the template DNA, stopping transcription (*8*).

More recently, actinomycin D was shown to bind with high affinity to single-stranded DNA (ssDNA) containing only dA, dT, and dG residues (*9*), confirming earlier reports suggesting possible drug-ssDNA interactions (*10*−*12*). Further confirmation of interactions with ssDNA was presented by Rill and Hecker (1996), who showed that actinomycin was highly effective in inhibiting HIV reverse transcriptase as well as DNA polymerases requiring a ssDNA template. Further, the drug was subsequently shown to recognize the sequence 5′-TAGT-3′ within a single strand of DNA (*13*) indicating a surprising sequence specificity for binding to ssDNA, although other studies have indicated that there may be a number of sites within ssDNA to which actinomycin binds with high affinity (*14*, *15*). Taken together, these studies have provided an additional model for the way in which actinomycin D may act as a potent inhibitor of transcription: not only by blocking the DNA ahead of RNA polymerase, but also by binding to the ssDNA in the open complex formed by the polymerase and preventing reannealing of ssDNA strands (*5*, *9*).

The nature of the complex between actinomycin D and ssDNA is important, inasmuch as (i) actinomycin may be the only small molecule known to interact preferentially with and have sequence specificity for ssDNA; (ii) the role of the pentapeptide rings of the drug may provide important information on the mechanism by which certain proteins recognize ssDNA (for example, the RecA protein or the HIV nucleocapsid protein); and (iii) the drug−ssDNA complex may yield clues to important DNA secondary structures occurring during transcription. Our previous reports (*13*, *16*) indicated that although the 5′-TAGT-3′ site in the R5 strand (Figure 1) was an important binding site, there was a length dependency on binding that was also critical. Particularly, shortening the R5 strand by 8 bases on the 3′ end decreased the binding affinity to 1/20th of that of the full-length strand. These data suggested that secondary structures might be important to the binding of the drug to ssDNA. To test this hypothesis, we undertook the experiments described in this report. Using the fluorescent analogue of actinomycin D (7-aminoactinomycin D), which has been shown to bind ssDNA, to bind dsDNA, and to have biological activity idential to that of actinomycin D (*9*, *17*−*20*), we demonstrate that even single base substitutions on the 3′ end of R5 can dramatically reduce the binding of the drug to ssDNA. We

* To whom correspondence should be addressed. Phone: (210)-677-3835. Fax: (210)-677-0058. E-mail: rwadkins@saci.org.

‡ Institute for Drug Development.

§ Los Alamos National Laboratory.

[1] Abbreviations: AMD, actinomycin D; 7AAMD, 7-aminoactinomycin D; MBN, mung bean nuclease; ssDNA, single-stranded DNA; dsDNA, double-stranded DNA.

S0006-2960(98)00973-8 CCC: $15.00
Published on Web 08/07/1998

```
R5:   5'- AAAAAAAAAATAGTTTTAAATATTT    -3'
R006: 5'- AAAAAAAAAATAGTTTTAAAAATTT    -3'
R007: 5'- AAAAAAAAAATAGTTTTAAATAATT    -3'
R008: 5'- AAAAAAAAAATAGTTTTAAATAAAT    -3'

HP1:  5'-    AAAAAAATAGTTTTAAATATTTTTTT-3'
HP1A: 5'-    AAAAAAATAATTTTAAATATTTTTTT-3'
HP2:  5'-      AAAAATAGTTTTAAATATTTTT  -3'
HP3:  5'-        AAATAGTTTTAAATATTT    -3'
HP4:  5'-          ATAGTTTTAAATAT      -3'
HP5:  5'-            TAGTTTTAAATA      -3'
HP6:  5'-              AGTTTTAAAT      -3'
```

FIGURE 1: Definition of single-stranded DNA.

further show that the sequence selectivity of AMD is due to binding and stabilization of metastable hairpin structures within ssDNA. Finally, we discuss the implications for the unusual biological activity of AMD.

MATERIALS AND METHODS

Materials. The oligonucleotides shown in Figure 1 were synthesized using standard solid-phase phosphoramidite chemistry on a Beckman Oligo 1000 DNA synthesizer. These oligos were >95% pure, as determined by ^{32}P end labeling with T4 polynucleotide kinase. For titration curves, the DNAs were used at this purity. For mung bean nuclease digestions (described below), the DNAs were run on a 20% denaturing polyacrylamide gel. The full-length bands were cut out of the gel and then eluted. The full-length DNAs were labeled at the 5′ end using [γ^{32}P]ATP (New England Nuclear, Boston, MA) and T4 polynucleotide kinase (New England Biolabs, Beverly, MA). The 7-aminoactinomycin D (7AAMD) was purchased from Fluka (Milwaukee, WI) and used without further purification. Mung bean nuclease was obtained from New England Biolabs. All other reagents were from standard commercial sources. Molar absorptivities for the ssDNAs were computed using the method of nearest-neighbor approximation (*21*). To determine concentrations, DNA absorbances were corrected for hyperchromicities measured at 70 °C.

Titration Curves. The binding of 7AAMD to the DNAs given in Figure 1 was determined using fluorescence spectroscopy. Fluorescence was excited at 530 ± 2 nm and emission collected at 630 ± 2 nm using an Aminco-Bowman AB2 spectrofluorometer. The titration buffer used for titrations was 20 mM Tris, 0.1 mM Na_2EDTA, pH 8.0. Background emission was subtracted from all values of the fluorescence. The 7AAMD was added to a continuously stirred buffer solution to a final concentration of 0.64 μM, and the initial fluorescence intensity of the drug at 630 nm was measured. Stock solutions of the DNAs in titration buffer were added to the drug solution, and the resulting fluorescence was measured. Additions were continued until apparent saturation was observed. Data were recorded as $\Delta F/F_o$, where ΔF is the difference in fluorescence at each DNA concentration from the initial fluorescence of the drug (F_o) and has units of μM^{-1}.

Fluorescence changes were fitted to the simple noninteracting site model of mass action. This model assumes a ligand (L) binds to a DNA site (D) according to:

$$L + D \rightleftharpoons LD$$

with a dissociation constant $K_d = ([L][D])/[LD]$. The values [L], [D], and [LD] are molar concentrations of the free ligand, free DNA sites, and ligand-bound DNA sites, respectively. The number of sites per DNA strand is given by:

$$[D] = n[D]_o$$

where $[D]_o$ is the concentration of DNA in strands, and n is the number of sites per strand. Fitting of data to the above model was done using the nonlinear least-squares function of Kaleidagraph (Synergy Software, Reading, PA) with n, K_d, and $\Delta F_{max}/F_o$ as adjustable parameters. Titrations were performed in triplicate, and the computed values of the parameters are reported in Table 2 for mean ± standard deviations of these triplicate determinations. For strands that reached saturation only at very high concentrations of added DNA, the number of sites per strand was fixed at 1 for curve fitting.

Thermal Denaturation. The melting of the DNAs in Figure 1 in the absence and presence of saturating amounts of 7AAMD was monitored using a 6-cell, temperature-regulated cell holder in a Beckman DU 640 UV−vis spectrophotometer. The Peltier device in this instrument allowed the collection of absorbances over the range 15−70 °C. For all DNAs shown in Figure 1, the melting was monitored by the change in absorbance at 260 nm for 5 different DNA concentrations, ranging in absorbance from ∼0.03 to ∼1.3 units. Absorbance changes were measured relative to the titration buffer controls in cuvette 1. For changes induced by 7AAMD, DNAs with absorbance ∼1.0 were melted in the presence of saturating amounts of 7AAMD (as determined from the titration curves described above). The absorbance changes at 260 nm were monitored with respect to cuvette 1, which contained only titration buffer and the equivalent concentration of 7AAMD. T_m values and $\Delta H°$ values for the melting data were determined by curve fitting according to the method of ref *22*.

Nondenaturing Gel Electrophoretic Analysis. A solution of ∼0.4 μM 5′-[^{32}P]-labeled DNA alone or mixed with 80 μM 7AAMD was allowed to sit at 4 °C for 30 min. A 2 μL aliquot of the solutions was mixed with 6 μL of 50% glycerol, and the samples were loaded on a 38 cm, 20% acrylamide gel (19:1 monomer−cross-linker) in Tris−borate−EDTA buffer (89 mM, 89 mM, 2 mM, respectively, pH 8.0). The gel was run at 300 V for 48 h at 4 °C. The positions of the DNAs with and without 7AAMD were visualized by autoradiography on Kodak BioMax film.

Mung Bean Nuclease Digestions. For this digestion, ∼0.4 μM 5′-[^{32}P]-labeled DNAs were incubated for 30 min with or without 80 μM 7AAMD in titration buffer. After 30 min, 20 units of mung bean nuclease (MBN) was added, the solution was vortexed, and digestion was continued for 2 min. A 2 μL aliquot of the 10 μL reaction solution was removed, placed into 8 μL of formamide, mixed, and immediately heated to 95 °C to stop the MBN digestion. Samples were cooled and loaded onto a 38 cm, 8 M urea, 20% denaturing polyacrylamide gel (19:1, acrylamide−bis acrylamide). The gel was run at 1800 V in Tris−borate−EDTA buffer for 3 h. The positions of the digested DNA were visualized by autoradiography on Kodak BioMax film.

Molecular Modeling of Hairpin Structures. A computer model of the hairpin formed from the sequence 5′-AGTTT-TAAATAT-3′ was built. The structure for the stem portion

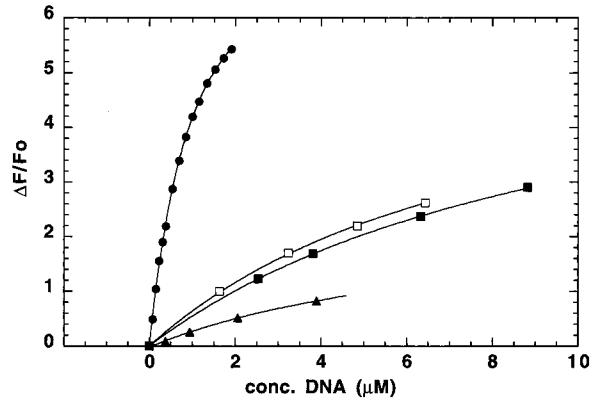

FIGURE 2: Titration of 7-aminoactinomycin D with R series single-stranded DNA. Data are shown as the fractional change in the original fluorescence of 0.6 μM 7-aminoactinomycin D with increasing concentrations of (●) R5, (▲) R006, (□) R007, and (■) R008. Solid lines indicate curve fits to the data, with the parameters recorded in Table 2.

of the hairpin was constructed using NAMOT2 (*23*, *24*). GA I and TT I types of mismatched base pairs as described by ref *25* were used for constructing the duplex. The duplex was constructed as that of a canonical B-DNA. To allow the backbone connection, twist angles for A1-G2 and T3-T4 steps were reduced from 36° to 26° and 8°, respectively. To introduce a cavity at the center of the helix for drug intercalation, the helical parameters (*26*) of the G2-T3 step were set to −0.8 Å, −0.6 Å, 6.5 Å, 0.0°, 20.0°, 0.0° for D_x, D_y, D_z, tilt, twist, and roll, respectively. The crystal structure of the actinomycin D complexed with a DNA oligomer (entry 173D in the Protein Data Bank) was used as the initial structure for the drug. The partial charges and atom types used for AMD were those reported earlier (*27*). The drug was docked into the cavity of the DNA duplex from the minor groove side as a rigid body with a short run of Metropolis Monte Carlo simulation (*28*). The drug−DNA (the stem portion) complex was then subjected to energy minimization using AMBER (*29*).

The structures of the loop portion of the hairpin were constructed using an algorithm specifically designed for modeling loops with fixed end-to-end distances (*30*). Random loop structures were first generated. Those structures with energies lower than a threshold (typically set at 10 000 kcal/mol) were selected for energy equilibration with a short run of Metropolis Monte Carlo simulation. Each of the energy-equilibrated structures was then subjected to energy minimization using AMBER. A pool of 500 energy-minimized loop structures were generated for hairpins with and without the drug.

RESULTS

Variations on the R5 Sequence. To understand the length dependence of AMD binding to the R5 sequence (*13*), we made single base pair changes in the R5 sequence to generate the sequences designated R006, R007, and R008 (Figure 1; note that these sequences are *not* those designated R6, R7, and R8 in ref *13*). Using the change in fluorescence intensity of 7AAMD in the presence of increasing concentrations of DNA, we were able to generate titration curves for the drug binding to the various sequences. The binding of 7AAMD to these sequences is shown in Figure 2, with data from the

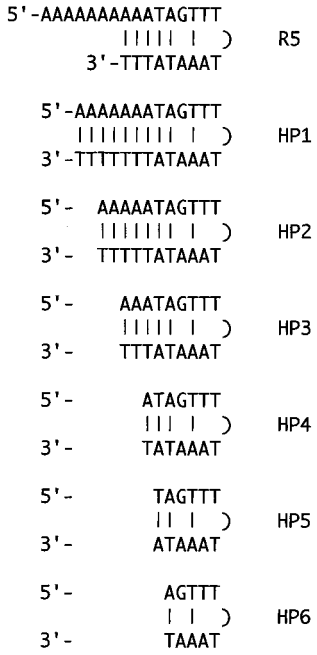

FIGURE 3: Hairpins derived from R5. The most likely secondary structure predicted from PCR primer analysis software is shown for R5. The HP series were derived from this predicted hairpin.

curve fits given in Table 2. These data are plotted as the fractional change in fluorescence intensity from the initial drug signal. New data for R5 are in excellent agreement with data reported earlier for the binding of 7AAMD to this sequence (*13*). Replacement of dT21 with dA (R006) abolished almost all affinity for this ssDNA (K_d > 10 μM). Further, the fluorescence enhancement observed with R006 was greatly diminished, indicating that this residue is key to formation of the drug−ssDNA complex. However, dT21 was not the only determinant of DNA binding. If dT21 was left in place, while dT23, dT24, or both was replaced with dA (R007, R008), both the binding affinity of 7AAMD and the fluorescence enhancement observed were also greatly reduced (Figure 2). These results suggested that a secondary structure in R5 was responsible for drug binding.

Analysis of the R5 sequence with the PCR primer analysis software *CPrimer* (Greg Bristol and Robert D. Andersen, School of Medicine, University of California, Los Angeles) revealed that the most likely stable secondary structure in R5 was a hairpin, shown in Figure 3, although no such hairpins were detected in the original work with AMD binding to ssDNA (*9*, *13*). Assuming the hairpin for R5 shown in Figure 3 was correct, we synthesized a series of ssDNAs that could form hairpins having different stabilities and that should maintain the binding site for AMD (Figure 3). These hairpins were designated HP1−HP6.

Thermal Characterization of Hairpins. The melting profiles for HP1−HP6 are shown in Figure 4. HP1−HP3 are shown to have pronounced sigmoidal melting profiles in the absence of drug, with accompanying hyperchromicities of ∼20%. HP4−HP6 showed reduced hyperchromicity in the range 15−70 °C (the limits of our apparatus), with no obvious sigmoidal shape to indicate melting. The apparent T_m values for melting of the hairpins were 34.2 ± 0.3, 28.9 ± 0.3, and 22.7 ± 0.5 °C for HP1, HP2, and HP3, respectively. The concentration dependence of T_m is shown in Figure 4B, and little or no dependence is observed. These

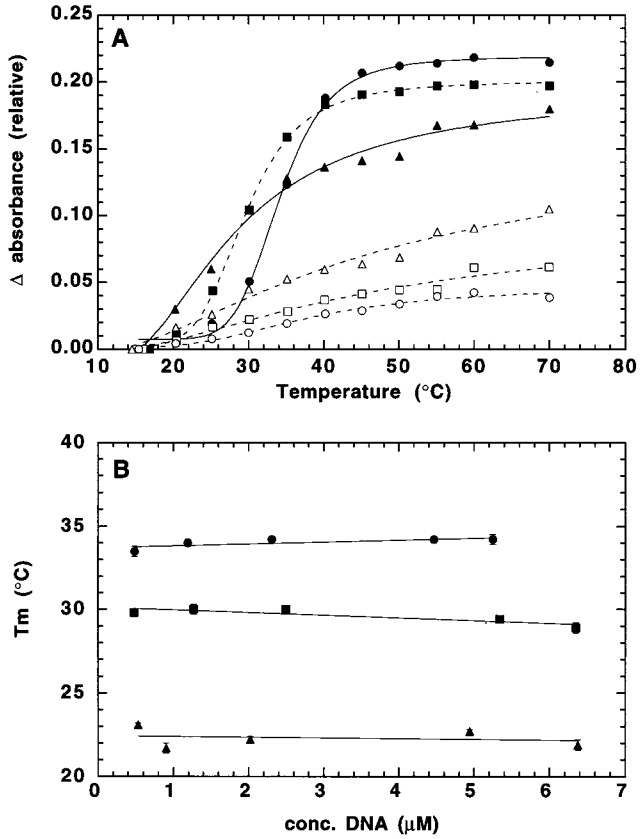

FIGURE 4: Thermal melting profile for HP series hairpins. (A) Fractional absorbance changes are shown for (●) HP1, (■) HP2, (▲) HP3, (△) HP4, (□) HP5, and (○) HP6. Derived values are recorded in Table 1. (B) Concentration dependence of T_m for (●) HP1, (■) HP2, and (▲) HP3.

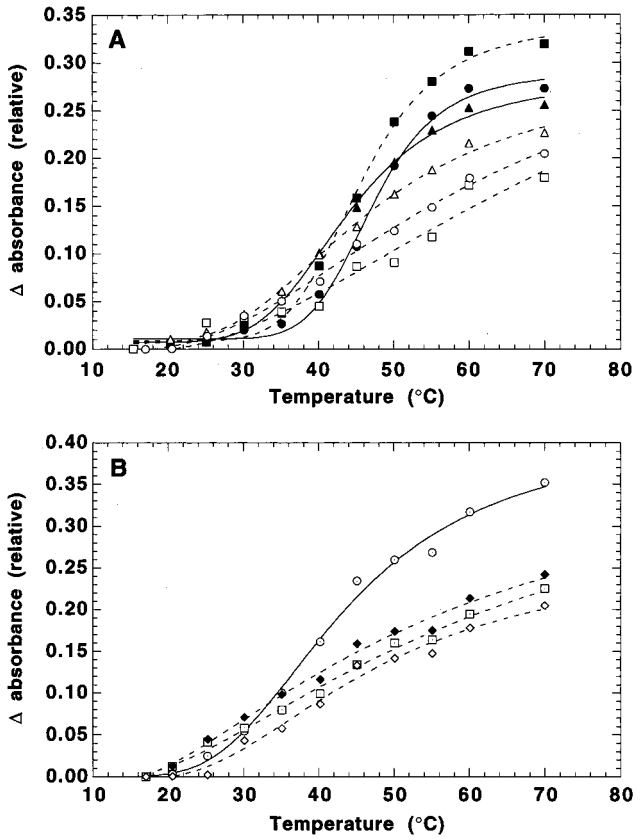

FIGURE 5: Shift in T_m induced by 7-aminoactinomycin D. (A) Fractional absorbance change at 260 nm relative to drug alone in buffer. Melting curves are shown for (●) HP1, (■) HP2, (▲) HP3, (△) HP4, (□) HP5, and (○) HP6 in the presence of saturating concentrations of 7-aminoactinomycin D. (B) Melting curves for (○) R5, (⊡) R006, (◆) R007, and (◇) R008 in the presence of saturating drug.

data suggested that HP1−HP3 indeed formed hairpins in solution. In contrast, HP4−HP6 and the R series of DNAs (including R5) showed no obvious melting in the temperature range examined, at any DNA concentration up to 8 μM. These data suggested that these latter DNAs are not in the form of hairpins above room temperature, in the absence of AMD.

The changes in melting profiles of the DNAs studied in the presence of saturating concentrations of 7AAMD are shown in Figure 5. In Figure 5A, the HP1−HP3 melting temperatures were shifted to ∼45 °C in the presence of 7AAMD (tabulated in Table 1). Only a minor dependence of the T_m value on hairpin stem length was observed due to the large free-energy contribution from drug binding (described below) as compared to that of hairpin formation. The $\Delta G°$ value for melting of the HP1 hairpin alone was only 2.0 kcal/mol, while the $\Delta G°$ for dissociation of the drug from HP1−HP3 was 10.8 kcal/mol.

HP3−HP6 also began to show distinct sigmoidal transitions with T_m around 45 °C but with significantly broader transitions and, consequently, lowered $\Delta H°$ values (Table 1). The melting of the R series in the presence of 7AAMD is given in Figure 5B, and a pronounced melting by R5 but significantly smaller transitions by R006, R007, and R008 were observed. This limited stabilization of R006, R007, and R008 reflected the low affinity of 7AAMD for these sequences as determined from the titration studies.

Nondenaturing Gel Electrophoretic Analysis. We also examined the ability of 7AAMD to alter the gel mobility of the HP and R series DNA. Figure 6 shows a nondenaturing, 20% acrylamide gel, with samples loaded with or without 7AAMD. No change in mobility was seen with any DNA in the presence of drug versus the no drug samples, in agreement with similar experiments performed earlier (*9*, *13*). However the mobilities of HP1, HP1A, HP3, HP4, and R5 were faster than would be expected on the basis of their length alone (see the inset in Figure 6). These data further indicated that these sequences do adopt hairpin conformations at temperatures below the T_m reported above (i.e., at 4 °C). However, the deviation of the mobility of R5 from the anticipated mobility of the fully linear DNA (dashed line in Figure 6 inset) is slight. This likely accounts for the earlier failure to note any difference in gel mobilities between R5 and other same-length ssDNAs that did not bind 7AAMD

Table 1: Melting Parameters for Single-Stranded DNA

DNA	T_m (°C)	$\Delta H°$ (kcal/mol)	T_m (°C) +7AAMD[a]	$\Delta H°$ +7AAMD[a] (kcal/mol)
HP1	34.2 ± 0.3	58.2 ± 4.7	46.9 ± 0.6	43.9 ± 4.7
HP2	28.9 ± 0.3	47.9 ± 5.7	45.3 ± 0.3	38.9 ± 2.1
HP3	22.7 ± 0.5	34.5 ± 7.6	43.5 ± 0.3	32.8 ± 1.4
HP4	<15		43.5 ± 0.5	22.5 ± 1.3
HP5	<15		52.7 ± 9.0	16.0 ± 7.8
HP6	<15		47.5 ± 1.8	16.1 ± 2.5
R5	<15		40.8 ± 1.3	22.6 ± 3.8

[a] Parameters determined in the presence of saturating concentrations of 7-aminoactinomycin D (DNA >99.9% drug bound).

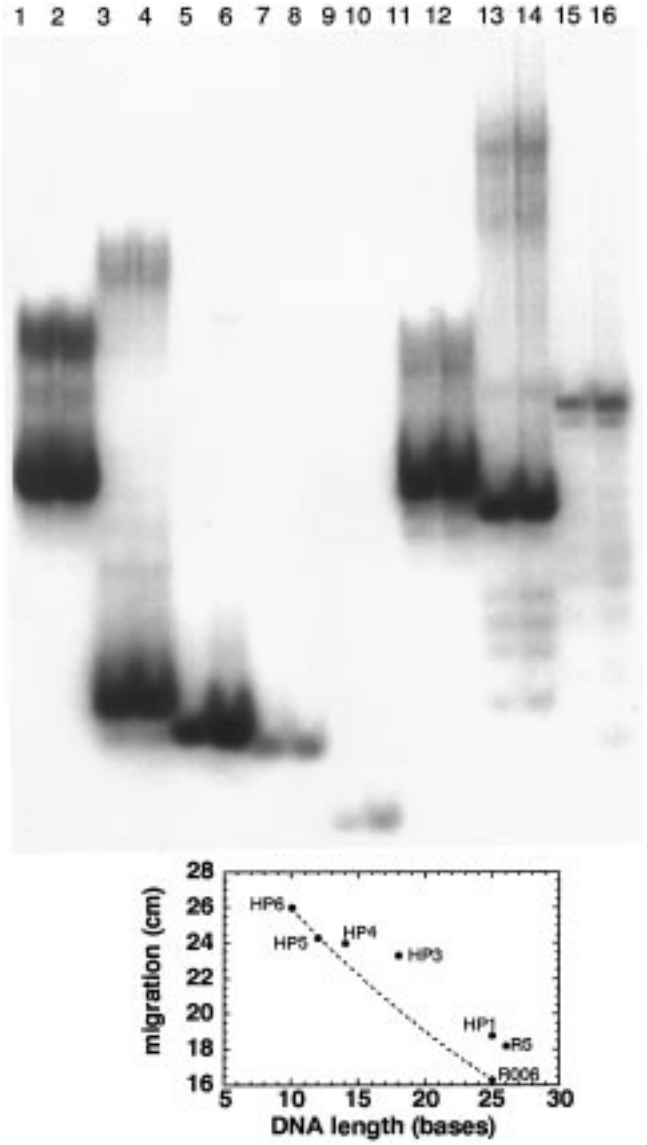

FIGURE 6: Mobility of DNAs in nondenaturing gels. Labeled DNAs ±80 μM 7AAMD were loaded in glycerol on a 20% acrylamide gel and run at 300 V at 4 °C for 48 h. Lanes shown are (1) HP1, (2) HP1 + 7AAMD, (3) HP3, (4) HP3 + 7AAMD, (5) HP4, (6) HP4 + 7AAMD, (7) HP5, (8) HP5 + 7AAMD, (9) HP6, (10) HP6 + 7AAMD, (11) HP1A, (12) HP1A + 7AAMD, (13) R5, (14) R5 + 7AAMD, (15) R006, and (16) R006 + 7AAMD. The inset graph indicates the mobility as a function of base length, with the dashed line fit through HP6, HP5, and R006 indicating the expected exponential mobility.

(*13*), as the shorter gels used in those studies were not sufficient to resolve slight differences.

Binding of 7AAMD to the HP Series. Representative titration curves for 7AAMD binding to the HPn series are shown in Figure 7, with the extracted binding parameters recorded in Table 2. HP1 bound 7AAMD more tightly than R5, with a K_d of 0.118 ± 0.025 μM. This was approximately a 10-fold higher affinity than that seen with R5 or other ssDNA described earlier (*9*, *13*). The increase in fluorescence intensity observed with the hairpins, while larger than that which has been seen with most dsDNA, was somewhat lower for HP1 than for the R series (Table 2). Similar binding parameters were observed for HP2 and HP3. HP1−HP3 appeared to bind 2 drugs/hairpin, as did the R5.

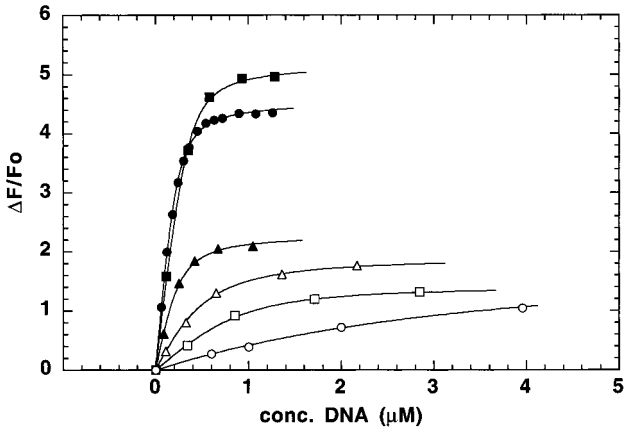

FIGURE 7: Binding of 7-aminoactinomycin D to the HP series of DNA. The fractional change in the original fluorescence of 0.6 μM 7-aminoactinomycin D is shown at increasing concentrations of (●) HP1, (■) HP2, (▲) HP3, (△) HP4, (□) HP5, and (○) HP6. Solid lines indicate curve fits to the data, with the parameters recorded in Table 2.

Table 2: Parameters for Binding of 7-Aminoactinomycin D to Single-Stranded DNA

DNA	$\Delta F/F_o$ (μM^{-1})[a]	n (sites/hairpin)	K_d (μM)
R5	11.75 ± 0.39	1.98 ± 0.48	1.148 ± 0.096
R006	4.08 ± 0.10	1[b]	12.77 ± 5.11
R007	9.61 ± 1.03	1[b]	8.49 ± 1.41
R008	9.66 ± 0.34	1[b]	9.59 ± 0.55
HP1	7.67 ± 0.94	2.95 ± 0.51	0.118 ± 0.025
HP2	7.82 ± 0.22	2.04 ± 0.20	0.089 ± 0.021
HP3	4.40 ± 0.70	2.51 ± 0.88	0.146 ± 0.061
HP4	3.56 ± 0.83	1[b]	0.200 ± 0.109
HP5	4.07 ± 1.95	1.08 ± 0.43	0.471 ± 0.386
HP6	4.00 ± 1.50	1[b]	0.391 ± 0.067

[a] Maximal change in fluorescence for 1 μM fully bound 7AAMD. [b] n value fixed at 1.00 for curve fitting.

For the HP4−HP6, the binding affinity dropped somewhat and the fluorescence enhancement for these strands was lowered. Further, the binding of HP4, HP5, and HP6 could be fitted with $n = 1$ site/hairpin, whereas with the HP1, HP2, and HP3, this was not possible. The reduced affinity, reduced fluorescence, and binding of 1 drug/hairpin coincided with the thermal stability of the hairpins. As described above, only HP1−HP3 were in the hairpin state under the conditions of the titration experiments.

Hairpin Cleavage by Mung Bean Nuclease. Mung bean nuclease (MBN) is a single-strand-specific nuclease which has been widely used to identify and characterize the loop regions of DNA hairpins (*31*−*34*). MBN is remarkably sensitive to the solvent accessibility of bases in the loop region in a hairpin. We used MBN to characterize the conformational changes in the HPn hairpins in the absence and presence of 7AAMD. Figure 8 shows the results of a brief MBN digestion of HP1 and HP3−HP6 with or without saturating amounts of 7AAMD. As a control, the strand HP1A (the HP1 sequence with the guanine replaced by adenine) was also examined.

In the absence of drug, cleavage of HP1 was most intense after dT14, dA15, and dA16 (Figures 8 and 9). These data suggested that, contrary to the designs in Figure 3, the loop region of HP1 was not the 5′-TTTA-3′ sequence, but rather the hairpin was shifted by one nucleotide. Further, the cleavage of HP1 revealed that while dA17 was protected

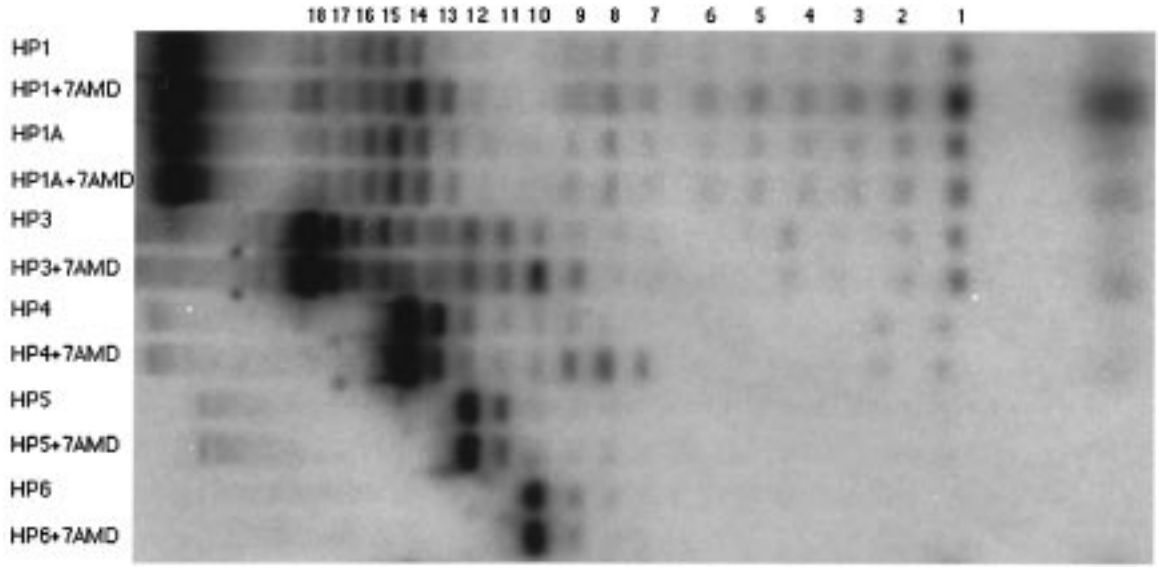

FIGURE 8: Mung bean nuclease digestion of HP series DNA. DNAs were ^{32}P-labeled at the 5′ end and digested with nuclease as described in the text. Samples marked +7AMD were incubated for 30 min at 23 ± 1 °C with 80 μM 7-aminoactinomycin D prior to digestion. The numbering scheme shown is from the 5′ end of the DNA.

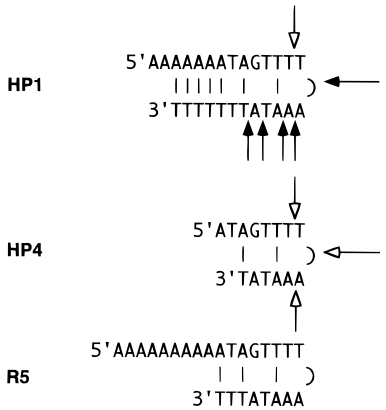

FIGURE 9: Summary of mung bean nuclease Digestion. The cleavage sites in the absence of drug, as determined from Figure 8, are shown for HP1 as solid arrows. The open arrows indicate the cleavage sites induced in HP1 and HP4 by the presence of 7-aminoactinomycin D. The deduced hairpin structures, and their likely occurrence in R5, are also shown.

from MBN digestion, the dT18 and dA19 were cleaved. This pattern of cleavage also occurred in the presence of 7AAMD; however, cleavage of the step between dT14 and dA15 was intensified in the presence of drug, while a new cleavage between dT13 and dT14 appeared. Note that the cleavage of HP1A was unaffected by the presence of 7AAMD.

An identical pattern of cleavage occurred with HP3 with or without 7AAMD (Figure 8), with the dT10−dA11 step being more intensely cleaved in the presence of drug, and a new drug-induced cleavage of the dT9−dT10 step. For HP4, no cleavage of the strand was seen in the absence of drug, but with 7AAMD cleavage after dT7, dT8, and dA9 was observed. These cleavage patterns are summarized in Figure 9. The lack of cleavage of HP4 in the absence of drug and no cleavage of HP5 or HP6 with or without drug indicated that these ssDNAs were not in hairpin conformation under the conditions of the digestion. Under conditions of limited digestion, MBN is much less efficient at cleaving linear ssDNA versus hairpin loop regions (*32*).

The results of the cleavage assay indicated an alternative hairpin loop to that given in Figure 2, as shown in Figure 9. For HP1−3, the 5′-AG-3′ step is bracketed by two T−T mismatches. HP4 would simply have an overhanging 5′ end (Figure 9), while HP5 and HP6 would have progressively shorter stem regions in any secondary structure stabilized by 7AAMD. The protection of dA17 in HP1 and dA13 in HP3 was consistent with this model, as this base is paired with a dT residue while the following T−A bases are not. The lack of cleavage in the 5′-TAGT-3′ stretch indicates that the dT and dG residues were likely stacked with the $(dA)_7$ stretch. Bases stacked with their neighbors are resistant to cleavage by MBN (*33*).

DISCUSSION

In this report, we have examined the sequence dependence of 7AAMD binding to ssDNA. By measuring the change in fluorescence intensity of the drug upon addition of DNA, the binding of the drug to ssDNA could be characterized. The 7AAMD was shown to bind to short ssDNA sequences (HP5 and HP6) that appear as linear DNA under the conditions examined. However, our data indicate that the high-affinity binding of 7AAMD to ssDNA ($K_d \sim 0.1$ μM) is to sequences with the ability to form unusual hairpins in a highly sequence-dependent manner. As indicated in Figure 9, the hairpins bound most tightly by AMD contain non-Watson−Crick base pairs, including an A−G mismatch and two T−T mismatches. This base-pairing scheme provides the unusual binding environment found in 7AAMD−ssDNA interactions (*9*, *13*). Stabilized structures containing non-Watson−Crick base pairs were also suggested to exist in other work on AMD−ssDNA interactions (*15*). The structure shown in Figure 9 also explains why replacing dT23 in R5 with dA (to give R007) reduced the binding affinity for 7AAMD. This thymidine residue is involved in the lone Watson−Crick base pair at the guanine binding site and likely is critical for stabilization of the adjacent mismatches.

The A−G mismatches are the components of a number of hairpin structures formed by polypurines in, for example, trinucleotide repeats associated with centromeric satillite DNA (*35*). However, to our knowledge, no data has been

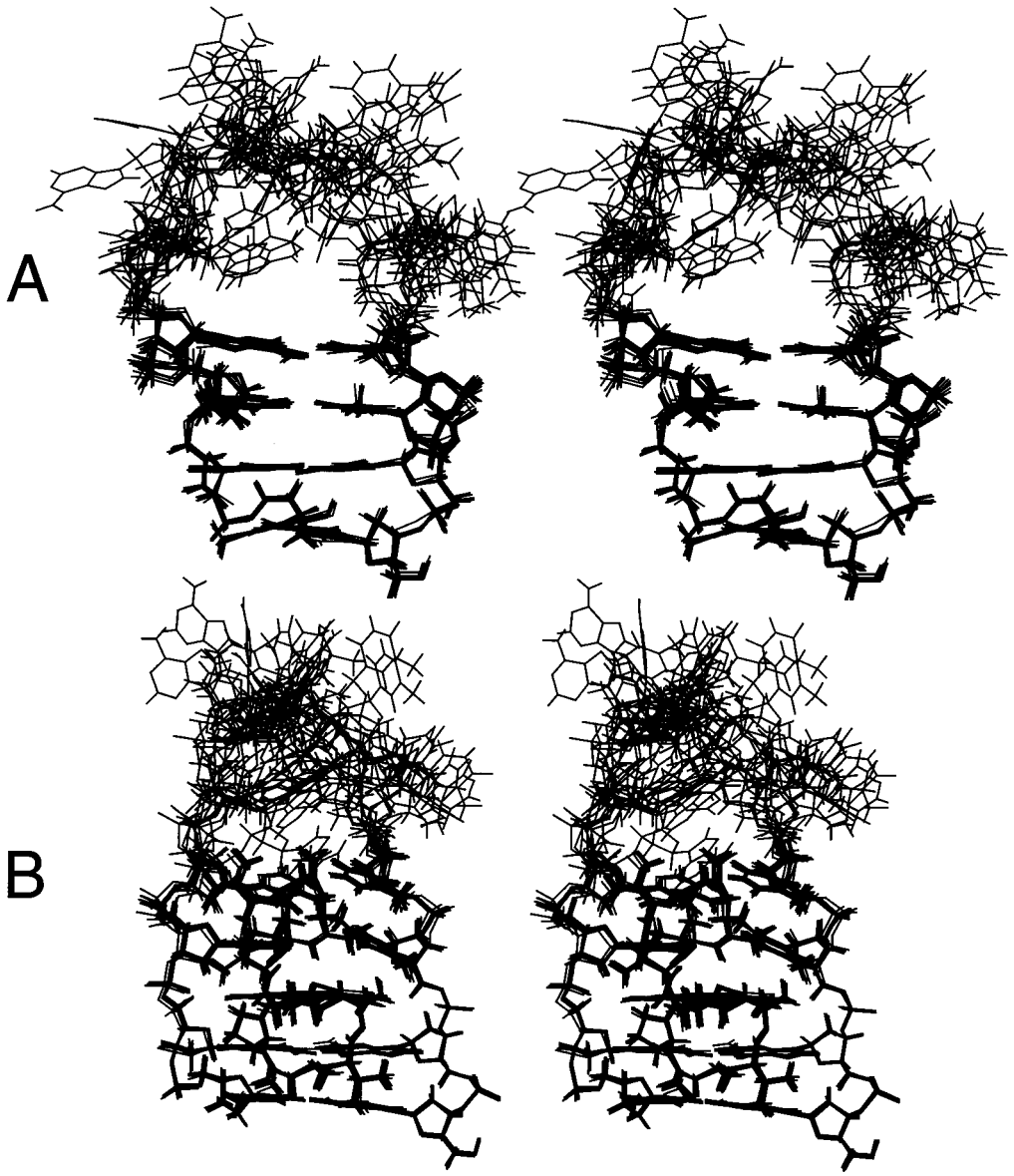

FIGURE 10: Molecular model of actinomycin D bound to hairpin motifs. Stereo diagrams of the superposition of the stem regions of the 10 lowest-energy hairpin structures formed from 5′-AGTTTTAAATAT-3′ are shown in part A. The superposition of the 10 lowest-energy structures when actinomycin D is intercalated between the GT step are shown in part B).

put forth characterizing the binding of AMD to A−G mismatches, so the exact nature of the drug−dG interaction is unclear at present. However, recent NMR experiments on AMD bound to cruciform structures in $(CAG)_n$ triplet repeats indicate that the drug can stabilize A−A mismatches on either side of a 5′-GC-3′ binding site (*36*). Further, the dual T−T mismatch has been shown previously to be a high-affinity binding site for AMD, when contained in dsDNA having a 5′-TGCT-3′ site (*37*). The fluorescence change noted for binding of 7AAMD to dsDNA with T−T mismatches (*37*) is remarkably similar to what we observed with R5 and HP1−3, suggesting that the 5-methyl groups of dT in these complexes protect the AMD chromophore from exposure to water. Since replacement of dT21 with dA (i.e., R006) eliminated binding of 7AAMD to the ssDNA, the hydrophobic pocket formed by the T−T mismatch is critical for drug recognition. Further, drug binding to the hairpin resulted in a perturbation in the loop region of the DNA, unstacking a dT residue from the "5′" end of the hairpin sequence. This indicated 7AAMD is able to induce significant conformational changes in the hairpins.

A tentative structural model that takes into account our experimental data is given in Figure 10. In Figure 10A, an overlay of hairpins constructed from the sequence 5′-AGTTTTAAATAT-3′ is shown, with the stem region of the 10 lowest-energy structures superimposed to show the configurational space accessible to the bases in the loop region. Base dT5 in these structures is somewhat less flexible than dT6, dA7, and dA8 and is consistent with the weak cleavage at this equivalent position by MBN in the absence of AMD (Figure 9). In Figure 10B, the hairpin model with AMD intercalated into the GT step of the sequence is shown as an overlay of the 10 lowest-energy structures. The pentapeptide backbone of the drug interacts with the loop region, where it could induce a conformational change in this area due to steric interactions. However, the flexibility of dT5 or the other bases in the loop region of these models does not deviate significantly from that in the absence of drug (as computed from mean-square deviation of the base coordinates), so it is not obvious why MBN

cleaves more strongly after dT5 in the drug−hairpin complex (Figures 8 and 9).

In the model of the AMD−hairpin complex, the T−T mismatches provide 2 methyl groups in the pseudo-major groove that would act to shield the chromophore from solvent, providing a hydrophobic environment for producing the increased fluorescence quantum yield and hypsochromic shift in the emission maximum of the drug. The α carbonyl oxygen of one AMD threonine interacts with the dG 2-amino moiety as is usually seen in the AMD−dsDNA complex (*38*, *39*). These models also suggest that the dA9 residue makes a bipartite base pair with both dT3 and dT4 residues, which may act to help stabilize the T−T mismatches. Additionally, while the dual T−T mismatches may be important for the 2 drugs/hairpin binding seen with R5 and HP1−3, it is not obvious from the model how 2 drugs could fit into this region of the DNA. However, other laboratories have shown that two AMD can bind both to a single 5′-GC-3′ site in dsDNA (*40*) as well as to the partially overlapping sites 5′-GCGC-3′ in dsDNA (*41*). Binding of 2 drugs to these sites resulted in significant curvature of the DNA so that both drugs were bound in the minor groove. More detailed information on the hairpin structure with and without AMD will require NMR experiments (currently underway) or crystal structure data.

The earlier literature reports on the binding of AMD to self-complementary hairpins (*42*) and cruciform DNA (*36*), as well as the work presented here on unusually stable hairpins containing non-Watson−Crick base pairs, indicates that these structures form very high affinity sites for AMD. The drug's affinity for hairpins and cruciforms is no doubt influenced by the "pocket" formed by the loop region, which can accommodate one of the pentapeptide rings of AMD (Figure 10B). The AMD−hairpin interactions also suggest a mechanism as to why AMD is such a potent inhibitor of transcription. During transcription in living cells, the DNA behind the RNA polymerase is highly negatively supercoiled (*43*). This supercoiled environment lends itself to stabilization of secondary structures in DNA, particularly of cruciform structures (*44*). The proneness of DNA behind RNA polymerase to form hairpins and/or cruciforms, coupled with the affinity for and stabilization of these structures by AMD, implies that these drug−hairpin complexes may be extremely stable in the cellular environment, and consequently, reannealing of template DNA strands after passage of the polymerase would be inhibited. The buildup of ssDNA behind the transcription complex would restrict the polymerase's continued travel and opening of dsDNA, effectively terminating transcription. Such a mechanism might work in addition to the drug's ability to directly block the passage of RNA polymerases. We are currently examining the ability of AMD to induce hairpins and/or cruciforms in DNA under conditions of supercoiling to test this proposed mechanism of drug action.

ACKNOWLEDGMENT

The authors would like to thank Dr. Thomas M. Jovin, Department of Molecular Biology, Max Planck Institute for Biophysical Chemistry, for his early encouragement on this project. We also thank Dr. Albert S. Benight, University of Illinois at Chicago, for helpful discussions.

REFERENCES

1. Waring, M. J. (1981) *Annu. Rev. Biochem. 50*, 159−162.
2. Goldberg, I. H., Beerman, T. A., and Poon, R. (1977) in *Cancer 5: A Comprehensive Treatise* (Becker, F. F., Ed) pp 427−456, Plenum, New York.
3. Goldberg, I. H., and Friedman, P. A. (1971) *Annu. Rev. Biochem. 40*, 775−810.
4. Kersten, H., and Kersten, W. (1974) in *Inhibitors of Nucleic Acid Synthesis*, pp 40−66, Springer, Berlin.
5. Sobell, H. M. (1985) *Proc. Natl. Acad. Sci. U.S.A. 82*, 5328−5331.
6. Straney, D. C., and Crothers, D. M. (1987) *Biochemistry 26*, 1987−1995.
7. White, R. J., and Phillips, D. R. (1988) *Biochemistry 27*, 9122−9132.
8. Müller, W., and Crothers, D. M. (1968) *J. Mol. Biol. 35*, 251−290.
9. Wadkins, R. M., and Jovin, T. M. (1991) *Biochemistry 30*, 9469−9478.
10. Green, C., and Tibbetts, C. (1981) *Nucleic Acids Res. 9*, 1905−1918.
11. Bunte, T., Novak, U., Friedrich, R., and Moelling, K. (1980) *Biochim. Biophys. Acta 610*, 241−247.
12. Reich, E. (1964) *Science 143*, 684−689.
13. Wadkins, R. M., Jares-Erijman, E. A., Klement, R., Rüdiger, A., and Jovin, T. M. (1996) *J. Mol. Biol. 262*, 53−68.
14. Hsieh, Y. L., Li, Y.-T., Henion, J. D., and Ganem, B. (1994) *Biol. Mass Spectrom. 23*, 272−276.
15. Rill, R. L., and Hecker, K. H. (1996) *Biochemistry 35*, 3525−3533.
16. Jares-Erijman, E. A., Klement, R., Machinek, R., Wadkins, R. M., Kankia, B. I., Marky, L. A., and Jovin, T. M. (1997) *Nucleosides Nucleotides 16*, 661−667.
17. Modest, E. J., and Sengupta, S. K. (1974) *Cancer Chemother. Rep. 58*, 35−48.
18. Chiao, Y.-C., Rao, K. G., Hook, J. W., Krugh, T. R., and Sengupta, S. K. (1979) *Biopolymers 18*, 1749−1762.
19. Gill, J. E., Jotz, M. M., Young, S. G., Modest, E. J., and Sengupta, S. K. (1975) *J. Histochem. Cytochem. 23*, 793−799.
20. Graves, D. E., and Wadkins, R. M. (1989) *J. Biol. Chem. 264*, 7262−7266.
21. Fasman, G. D., Ed. (1975) *CRC Handbook of Biochemistry and Molecular Biology*, 3rd ed, Vol. I, p 589, Chemical Rubber Publishing Co., Cleveland, OH.
22. Marky, L. A., and Breslauer, K. J. (1987) *Biopolymers 26*, 1601−1620.
23. Carter, E. S., and Tung, C.-S. (1996) *Comput. Appl. Biosci. 12*, 25−30.
24. Tung, C.-S., and Carter, E. S. (1994) *Comput. Appl. Biosci. 10*, 427−433.
25. Hobza, P., and Sandorfy, C. (1987) *J. Am. Chem. Soc. 109*, 1302−1307.
26. Tung, C.-S., Soumpasis, D. M., and Hummer, G. (1994) *J. Biomol. Struct. Dyn. 11*, 1327−1344.
27. Lybrand, T. P., Brand, S. C., Creighton, S., Shafer, R. H., and Kollman, P. A. (1986) *J. Mol. Biol. 191*, 495−507.
28. Metropolis, N., Rosenbluth, A. W., Rosenbluth, M. N., Teller, A. H., and Teller, E. (1953) *J. Chem. Phys. 21*, 1087−1092.
29. Weiner, S. J., Kollman, P. A., Nguyen, D. T., and Case, D. A. (1986) *J. Comput. Chem. 7*, 230−252.
30. Tung, C.-S. (1997) *Biophys. J. 72*, 876−885.
31. Xodo, L. E., Manzini, G., Quadrifoglio, F., Marel, G.v.d., and Boom, J.v. (1991) *Nucleic Acids Res. 19*, 1505−1511.
32. Kabotyanski, E. B., Zhu, C., Kallick, D. A., and Roth, D. B. (1995) *Nucleic Acids Res. 23*, 3872−3881.
33. Baumann, U., Frank, R., and Blöcker, H. (1986) *Eur. J. Biochem. 161*, 409−413.
34. Baumann, U., and Chang, S. (1996) *Mol. Biol. Rep. 22*, 25−31.
35. Huertas, D., and Azorín, F. (1996) *Biochemistry 35*, 13125−13135.
36. Lian, C., Robinson, H., and Wang, A. H.-J. (1996) *J. Am. Chem. Soc. 118*, 8791−8801.

37. Liu, C., and Chen, F.-M. (1996) *Biochemistry 35*, 16346−16353.
38. Kamitori, S., and Takusagawa, F. (1992) *J. Mol. Biol. 225*, 445−456.
39. Jain, S. C., and Sobell, H. M. (1972) *J. Mol. Biol. 68*, 1−20.
40. Zhou, N., James, T. L., and Shafer, R. H. (1989) *Biochemistry 28*, 5231−5239.
41. Chen, H., Liu, X., and Patel, D. J. (1996) *J. Mol. Biol. 258*, 457−479.
42. Chen, F.-M., Jones, C. M., and Johnson, Q. L. (1993) *Biochemistry 32*, 5554−5559.
43. Liu, L. F., and Wang, J. C. (1987) *Proc. Natl. Acad. Sci. U.S.A. 84*, 7024−7027.
44. Palecek, E. (1991) *Crit. Rev. Biochem. Mol. Biol. 26*, 151−226.

BI9809730